AGU ADVANCING EARTH AND SPACE SCIENCE

Geophysical Research Letters®

RESEARCH LETTER
10.1029/2022GL099229

Key Points:

- Hot plasma effects are analyzed and parameterized using analytical equations for observed electromagnetic ion cyclotron (EMIC) waves
- Hot plasma parametric model agrees very well with numerical results and can be implemented to evaluate diffusion coefficients more precisely
- Hot plasma effects may decrease the minimum resonant energy of electrons for high-frequency EMIC waves

Correspondence to:
M. F. Bashir,
frazbashir@epss.ucla.edu

Citation:
Bashir, M. F., Artemyev, A., Zhang, X.-J., & Angelopoulos, V. (2022). Hot plasma effects on electron resonant scattering by electromagnetic ion cyclotron waves. *Geophysical Research Letters*, *49*, e2022GL099229. https://doi.org/10.1029/2022GL099229

Received 22 APR 2022
Accepted 17 MAY 2022

Hot Plasma Effects on Electron Resonant Scattering by Electromagnetic Ion Cyclotron Waves

M. Fraz Bashir[1], Anton Artemyev[1,2], Xiao-Jia Zhang[1], and Vassilis Angelopoulos[1]

[1]Earth, Planetary, and Space Sciences, University of California, Los Angeles, Los Angeles, CA, USA, [2]Space Research Institute, RAS, Moscow, Russia

Abstract Resonant scattering by electromagnetic ion cyclotron (EMIC) waves is one of the most effective mechanisms of relativistic electron losses in Earth's inner magnetosphere. Low-altitude spacecraft measurements, however, often show that the energy range of precipitating electrons is wider than theoretical predictions based on the cold plasma dispersion of EMIC waves. To explain this discrepancy, we examine the diffusion rates of EMIC waves by including hot plasma effects in their dispersion relation. Using the observed ion distribution functions, we investigate the hot plasma effects on the EMIC wave dispersion for a wide frequency range. We develop analytical equations for hot plasma effects on EMIC dispersion, and apply this model to diffusion rate evaluations. We show that hot ion effects tend to increase the minimum resonant energy for the frequency range around wave intensity maxima, but can decrease the minimum resonant energy for the higher-frequency part of wave spectra.

Plain Language Summary Quantification of dynamics of relativistic electron fluxes in the Earth's radiation belts is one of the main problems of space plasma physics. Resonance of such relativistic electrons with electromagnetic ion cyclotron (EMIC) waves is considered to provide a very effective electron scattering into the Earth's atmosphere. Energies of electrons resonating with EMIC waves for typical wave characteristics and background plasma conditions rarely fall below 1 MeV, and most of the observed EMIC waves are believed to scatter and precipitate ultra-relativistic electrons. Conjugate observations from near-equatorial and low-altitude spacecraft, however, often show near-equatorial EMIC waves correlated with precipitation of sub-MeV electrons below the minimum resonant energy. Such a decrease in resonant energy can be attributed to hot ion contribution to EMIC wave properties. This paper provides a generic hot plasma model which agrees well with the exact numerical solution and highlights the importance of hot plasma effects on the relativistic electron scattering by EMIC waves for a wide range of plasma parameters.

1. Introduction

Relativistic electron losses in the inner magnetosphere are mainly attributed to magnetopause shadowing due to outer radial diffusion (e.g., Shprits et al., 2006; Sorathia et al., 2018; Turner et al., 2012) and electron scattering into the atmosphere due to their resonant interaction with various electromagnetic waves (e.g., Millan & Thorne, 2007, and references therein). The most effective wave mode responsible for such a scattering is electromagnetic ion cyclotron (EMIC) waves (Thorne & Kennel, 1971). The EMIC wave intensity is often sufficiently high to provide fast electron scattering in quasi-linear diffusion or (Drozdov et al., 2017; Ni et al., 2015) nonlinear resonant interactions (Albert & Bortnik, 2009; Grach & Demekhov, 2020; Kubota et al., 2015). The good correlation between low-altitude measurements of relativistic electron precipitation and near-equatorial EMIC wave measurements supports the hypothesis that EMIC waves play a key role in relativistic electron losses from the Earth's radiation belts (Blum et al., 2015; Capannolo, Li, Ma, Shen, et al., 2019; Zhang et al., 2021).

Resonant energies of electrons interacting with EMIC waves are well determined by the cold plasma dispersion (Bashir & Ilie, 2018; Summers & Thorne, 2003) and for typical H- and He-band waves this energy is usually larger than 1 MeV (Ni et al., 2015). Therefore, multiple observations of EMIC wave scattering of sub-MeV electrons (e.g., Capannolo, Li, Ma, Chen, et al., 2019; Hendry et al., 2017) pose questions for models of EMIC wave resonances with such electrons. Besides the effects of nonresonant electron scattering (Chen et al., 2016) and the resonance broadening due to high wave amplitude (see discussion in Cai et al., 2020; Karimabadi et al., 1992), the most possible solution to this puzzle is the inclusion of hot plasma effects in the EMIC wave dispersion, because EMIC waves are indeed often observed in association with energetic ion injections from the

magnetotail (e.g., Jun et al., 2019) and such ion populations may significantly modify the EMIC dispersion (X. Cao et al., 2020; Chen et al., 2011; Silin et al., 2011; Yoon et al., 2011). It has been reported, however, that hot plasma effects for observed EMIC waves only result in an increase in the energy of resonant electrons (J. Cao et al., 2017; Chen et al., 2019). But these estimates were focused on EMIC wave frequencies corresponding to the peak wave intensity, whereas low-intensity higher-frequency part of EMIC waves may be more promising to scatter sub-MeV electrons (Bashir et al., 2022; Denton et al., 2019; Zhang et al., 2021). This study aims to reveal and model the hot plasma effects for relativistic electron scattering by observed EMIC waves.

We analyze the hot plasma effects on relativistic electron resonant scattering based on three EMIC events observed by the Time History of Events and Macroscale Interactions during Substorms (THEMIS) spacecraft (Angelopoulos et al., 2008) and develop a hot plasma model applicable to a wide range of plasma parameters in the Earth's magnetosphere. Section 2 describes the data set, spacecraft instruments, and the analysis of EMIC wave events for the observed ion and wave characteristics. Based on observed EMIC waves and plasma properties, the hot plasma effects on the EMIC wave dispersion are analyzed in Section 3 by numerically solving the dispersion relation for EMIC waves. An analytical hot plasma model is then generalized and compared with numerical solutions in Section 4. We show that the hot plasma model agrees very well with numerical results for a wide range of plasma parameters and thus can be used to estimate pitch angle diffusion rates in radiation belt diffusion models and test particle simulations. The pitch angle diffusion rates for the observed parameters are estimated in Section 5, which demonstrate that the presence of hot plasma significantly changes the scattering rates. The main results are summarized in Section 6.

2. THEMIS Observations: Data Set and Event Analysis

We use measurements in the inner magnetosphere and near-Earth plasma sheet from two probes (A and E) of THEMIS (Angelopoulos, 2008) mission, which are ideal for capturing EMIC waves in the near-equatorial magnetosphere. We use magnetic field data from Flux Gate Magnetometer (FGM) (Auster et al., 2008). In the fast mode, FGM measures waveforms at a sufficiently high time resolution (1/4 s before July 2015 and 1/16 s afterward) to cover the EMIC wave frequency range at $L > 6$. We will also use THEMIS electrostatic analyzer (ESA) (McFadden et al., 2008) measurements for <25 keV ion distribution functions with pitch-angle and energy resolutions sufficient to investigate EMIC wave dispersion (Bashir et al., 2022). The cold plasma density is inferred from the spacecraft potential measurements (Nishimura et al., 2013) and the L-shell values are calculated using the dipole magnetic field model.

We have selected three events with EMIC waves as shown by the overview plots in Figure 1; Gaussian fittings to the observed ion distributions and wave spectra are further shown in Figure 2. Figure 1 depicts that all three events are field-aligned EMIC waves with left-handed polarization and accompanied by anisotropic ion distributions. For all three events, we have three ion populations consisting of cold, warm and energetic ions over a wide range of plasma and wave spectrum parameters, as shown in Figure 2 (top). Plasma and wave characteristics for these three events will be used to test our model of the hot plasma effects on the EMIC wave dispersion.

3. Hot Plasma Dispersion Effects

The generalized dispersion relation for parallel propagating EMIC waves in the presence of cold and hot anisotropic ion populations (following Chen et al. (2011)) can be written as.

$$D(\omega,k)=\frac{x^2}{f^2}\frac{m_e}{m_p}-y^2-x+\sum_{cs}\frac{x\eta_{cs}}{1-\epsilon_{cs}x}+\sum_{hs}\eta_{hs}\left[A_{hs}+\left(A_{hs}+\frac{x}{\epsilon_{hs}x-1}\right)\xi_{hs}\mathcal{Z}\right]=0 \quad (1)$$

where the subscript e, cs, and hs represent the cold electrons, cold ion populations, and hot ion populations, respectively. $x=\omega/\Omega_p=\Re\omega/\Omega_p+i\gamma/\Omega_p$ is the normalized complex frequency, with $\Re\omega$ being the real frequency and γ the growth rate, $y=ck_{\parallel}/\omega_{pi}$ is the normalized field-aligned wavenumber and $f=\omega_{pe}/\Omega_e$ represents the electron plasma frequency to gyro frequency ratio with $\omega_{(pe,pi)}=\sqrt{n_{0e}e^2/\left(\epsilon_0\left(m_e,m_p\right)\right)}$ and $\Omega_{(e,p)}=eB_0/m_{(e,p)}$. B_0 is the ambient magnetic field, m_e; m_p are the mass of an electron and proton; n_{0e} is the electron density which satisfies the quasi-neutrality condition ($n_{0e}=\sum_{cs}n_{cs}+\sum_{hs}n_{hs}$), where n_{cs} and n_{hs} represent the density of cold and

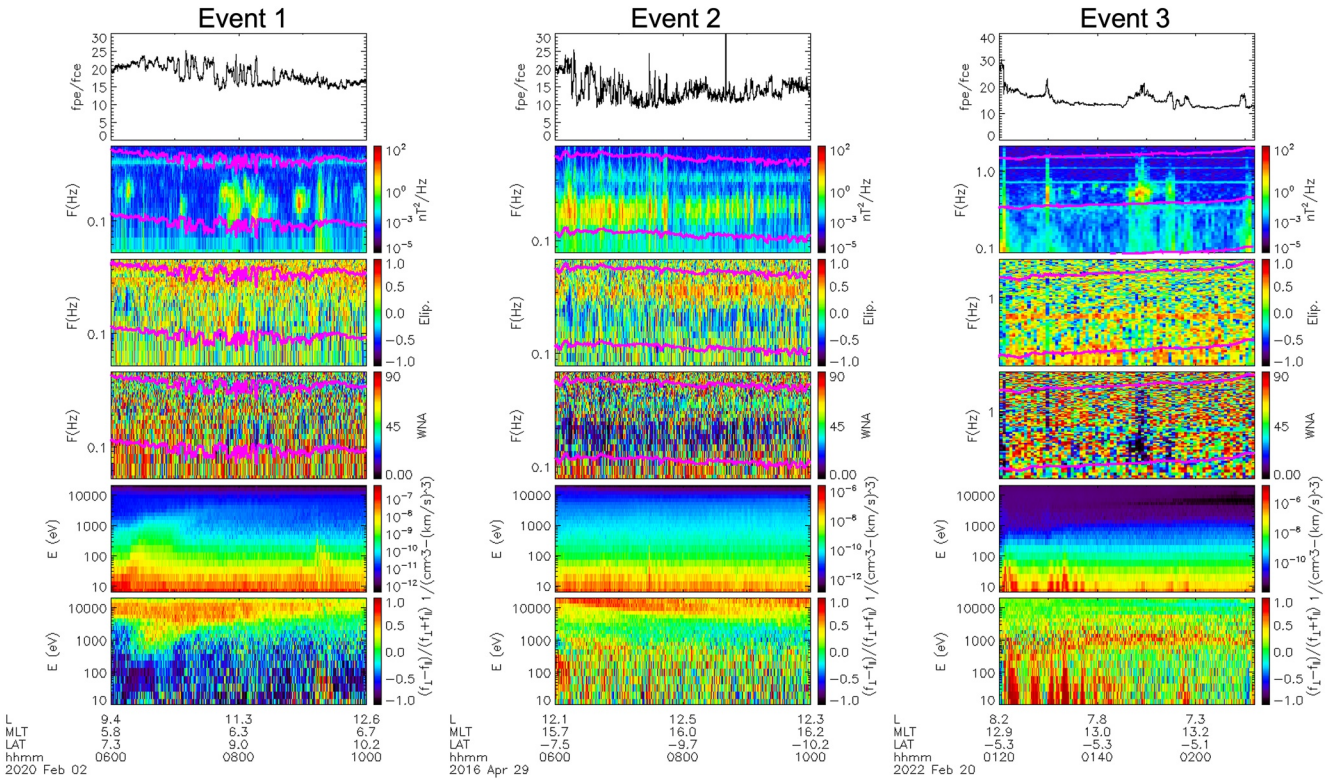

Figure 1. Overview of three electromagnetic ion cyclotron wave events captured by Time History of Events and Macroscale Interactions during Substorms (THEMIS). Each set of panels from top to bottom show the f_{pe}/f_{ce}, magnetic wave power, ellipticity, wave normal angle (WNA), ion omnidirectional flux and ion flux anisotropy $(f_\perp - f_\parallel)/(f_\perp + f_\parallel)$. The proton and helium cyclotron frequencies are shown by the curves f_{cp} (top) and f_{cHe} (bottom) in the wave panels respectively. Event 1 and 3 are observed at THEMIS-A and Event 2 is taken from THEMIS-E probes.

hot ion populations, respectively. The fractional ion composition is defined as $\eta_{(cs,hs)} = n_{(cs,hs)}/n_{0e}$ and fractional mass as $\epsilon_{(cs,hs)} = m_{(cs,hs)}/m_p$. The temperature anisotropy is defined as $A_{(hs)} = T_{hs\perp}/T_{hs\parallel} - 1$ for additional ion populations, with $T_{hs\perp}$ and $T_{hs\parallel}$ being the temperature in the perpendicular and parallel directions with respect to the magnetic field. $\mathcal{Z} = \mathcal{Z}(\xi_{hs})$ is the usual plasma dispersion function (Fried & Conte, 1961) with the argument $\xi_{hs} = (x - 1/\epsilon_{hs}) / \left(y\sqrt{\beta_{hs\parallel}}\right)$, where $\beta_{hs\parallel} = (2T_{hs\parallel}/m_{hs})/v_A^2$ and $v_A = B_0/\sqrt{\mu_0 m_p n_{0e}}$ is the Alfven speed. Note that the last term related to the hot plasma contains contributions from both warm and energetic ion populations. The number of additional hot ions and their energy will be determined from particle measurements from THEMIS.

In these dimensionless variables, the minimum resonant energy of electrons resonating with EMIC waves is given by Chen et al. (2011)

$$E_{\min} = \left(\sqrt{1 + \frac{m_p}{m_e}\frac{1}{f^2 y^2}} - 1\right) m_0 c^2 \tag{2}$$

For a fixed wave frequency, this equation shows that a larger wavenumber corresponds to smaller energies of electrons resonating with EMIC waves.

4. Hot Plasma Model for EMIC Waves

In order to model and parameterize the hot plasma effects, we will obtain the analytical expression for field-aligned wavenumber $k_\parallel$ with hot plasma corrections. We, therefore, expand the plasma dispersion function in the large argument limit, that is, $\xi_{(hs)} \gg 1$, by keeping the higher order thermal effects resulting in $Z(\xi_{hs}) = -\xi_{hs}^{-1}\left(1 + \xi_{hs}^{-2}/2\right) + i\sqrt{\pi}\exp\left[-\xi_{hs}^2\right]$ and after some simple mathematical steps for the weakly

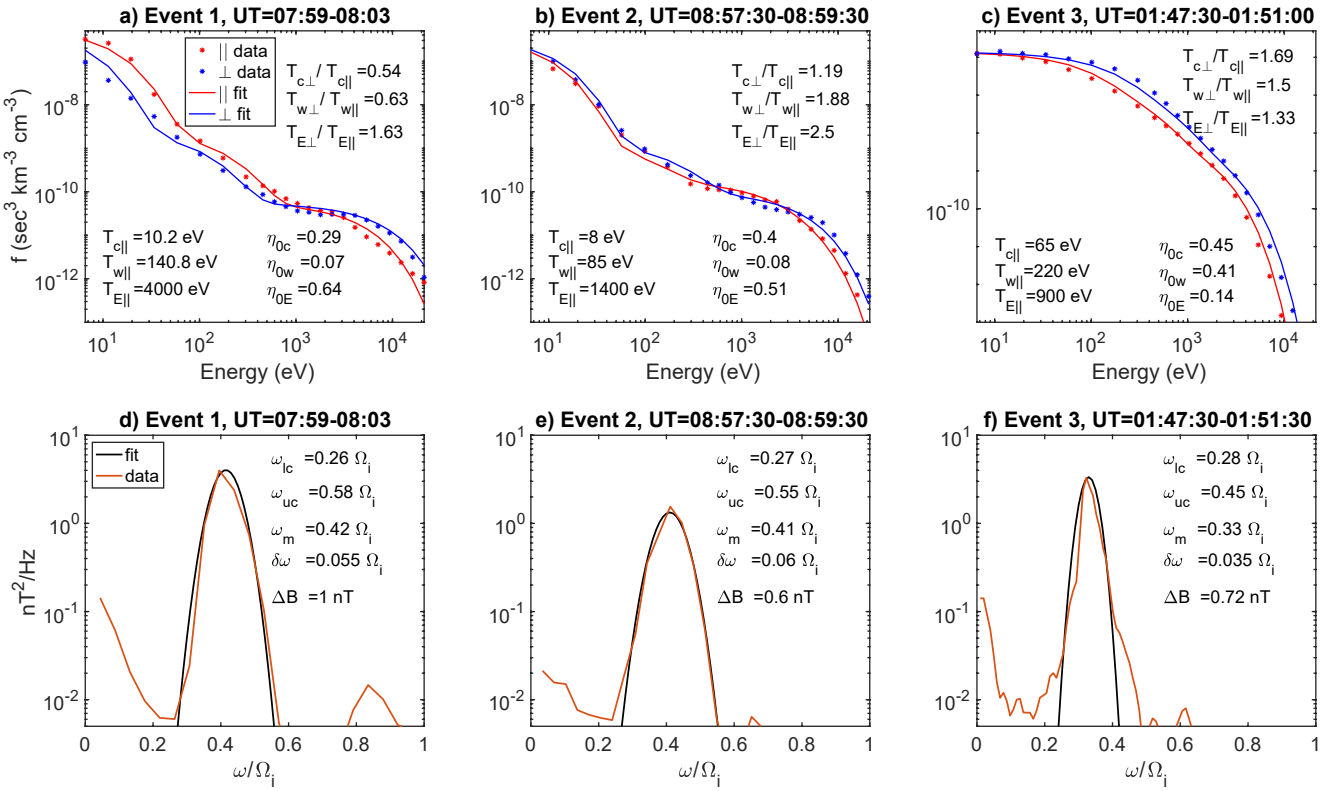

Figure 2. (a–c) Fitted ion distribution functions consisting of cold, warm, and energetic protons (top panels) and (d–f) electromagnetic ion cyclotron (EMIC) wave spectrum (bottom panels) during the three EMIC events from Figure 1: fitted parameters are inserted in each panel respectively.

growing condition, that is, $\gamma \ll \Re\omega$, we obtain the analytical expressions for the EMIC wave growth rate $\gamma = -D_i/(\partial D_r/\partial\omega_r)$ by using real and imaginary parts of the dispersion relation Equation 1 as given by

$$D_r(\omega_r, k_\parallel) = -y^2 + \frac{x^2}{f^2}\frac{m_e}{m_p} - x + \sum_{cs}\frac{x\eta_{cs}}{1-\epsilon_{cs}x} + \sum_{hs}\eta_{hs}\left[A_{hs} - \left(A_{hs} + \frac{x}{\epsilon_{hs}x-1}\right)\left(1 + \frac{1}{2\xi_{hs}^2}\right)\right] \quad (3)$$

and

$$D_i(\omega_r, k) = -\sqrt{\pi}\sum_{hs}\eta_{hs}\xi_{hs}\left(A_{hs} + \frac{x}{\epsilon_{hs}x-1}\right)\exp\left[-\xi_{hs}^2\right] \quad (4)$$

and EMIC waves dispersion relation $D_r(\omega_r, k_\parallel) = 0$ simplified to

$$y^2 = \frac{\frac{x^2}{f^2}\frac{m_e}{m_p} - x + \sum_{cs}\frac{x\eta_{cs}}{1-\epsilon_{cs}x} + \sum_{hs}\frac{x\eta_{hs}}{1-\epsilon_{hs}x}}{1 + \sum_{hs}\eta_{hs}\left[\left(A_{hs} + \frac{x}{\epsilon_{hs}x-1}\right)\left(\frac{\beta_{hs\parallel}}{2(x-1)^2}\right)\right]} \quad (5)$$

Using Equation 5, we obtain the wavenumber ratio of hot plasma to cold plasma as

$$\frac{k_{hot}}{k_{cold}} = \left[1 + \sum_{hs}\eta_{hs}\left\{\left(A_{hs} + \frac{x}{\epsilon_{hs}x-1}\right)\left(\frac{\beta_{hs\parallel}}{2(x-1)^2}\right)\right\}\right]^{-1/2} \quad (6)$$

The hot plasma effects on EMIC properties and minimum resonant energies and their comparison with the cold plasma results are presented in Figure 3 based on observed plasma parameters (see Figure 2) during three EMIC wave events. We note that for all events, the hot plasma effects decrease the wavenumber at lower frequencies

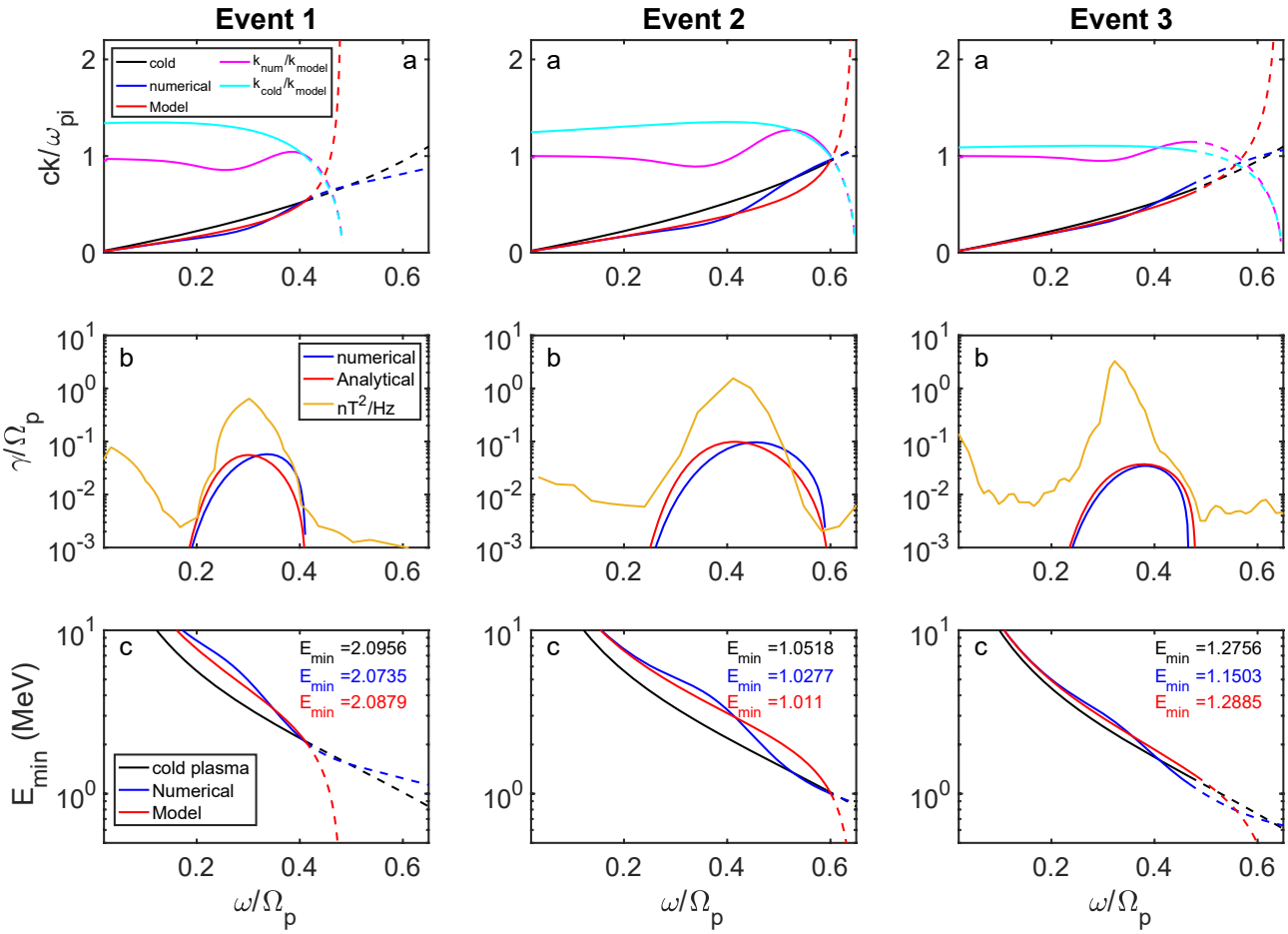

Figure 3. Comparison of the numerical and analytical model for the observed electromagnetic ion cyclotron (EMIC) wave events based on ion distribution fits from Figure 2. In top panels (a), we show the normalized wave number ck/ω_{pi} as a function of normalized frequency ω/Omega$_p$ for the cold plasma (black). For the hot plasma case, we present results from the numerical solution (blue) and analytical model (red), respectively. The ratios of numerical to analytical model wave number k_{num}/k_{model} and cold to hot plasma wave number k_{cold}/k_{model} are shown in magenta and cyan colors, respectively. The growth rate comparison for numerical and analytical cases is presented in panels (b), with the observed EMIC wave power (nT^2/Hz) overlaid. The minimum resonant energy (E_{min}) as a function of the normalized frequency ω/Ω_p is shown in panels (c). The solid curves show the range of frequencies for which the wave growth rate is positive and dashed curves show the results for the extended frequency range.

which results in a higher minimum resonant energy (E_{min}). For higher frequencies, the wavenumber can either approach or exceed the cold plasma result based on ion distributions; the highest frequency of the observed EMIC wave brings E_{min} either down to or even lower than the result from the usual cold plasma dispersion. The wavenumber decrease (E_{min} increase) for the frequency of maximum wave power is a well-known effect of hot plasma (e.g., J. Cao et al., 2017; Chen et al., 2019). Figure 3, however, demonstrates that hot plasma effects can lower E_{min} as close to the cold plasma result (see Event 1, panel c) or even lower than that (see Events 2 and 3, panel c) for the highest frequencies of positive growth rate (i.e., more marginally stable waves that have a finite intensity in observations).

Figure 3a shows that our analytical hot plasma model Equation 6 agrees very well (i.e., within 10%–15% error) with the numerical results for the wavenumber estimation and also the growth rate and instability threshold (maximum possible frequency with $D_i \geq 0$). The instability threshold actually determines the maximum EMIC frequency available for k_{hot}/k_{cold} evaluations. This parameter may be determined directly from the analysis of the observed wave spectrum.

5. Pitch Angle Scattering of Relativistic Electrons Based on the Hot Plasma Model

To quantify the hot plasma effects described by the model Equation 6 for relativistic electron scattering by EMIC waves and to estimate the corresponding resonant electron energy range, we apply the analytical approximation Equation 6 to quasi-linear diffusion equations. The local pitch angle diffusion coefficient for field-aligned EMIC waves, $D_{\alpha\alpha}$, is given by Summers (2005), Ni et al. (2018)

$$D_{\alpha\alpha} = \frac{\pi}{2}\frac{\Omega_e^2}{W_0}\frac{1}{(E_k+1)^2}\left(1-\frac{\omega\mu}{kv}\right)^2\frac{W(k)}{|v\mu - d\omega/dk|}, \tag{7}$$

where Ω_e is the electron cyclotron frequency, $W_0 = B_0^2/8\pi$ is the magnetic energy density of the background magnetic field, and E_k is the dimensionless particle kinetic energy given by $E_k = \gamma - 1$ with γ being the relativistic Lorentz factor. ω and k represent the frequency and wavenumber of parallel propagating EMIC waves. The wavenumber $k(\omega)$ and the group velocity $|d\omega/dk|$ are calculated from the cold plasma dispersion relation with the correction given by model Equation 6, the resonant velocity v is obtained from the resonant condition of EMIC waves with relativistic electrons, that is, $\omega - v\mu k = -\Omega_e/\gamma$ and $\mu = \cos\alpha$, with α being the pitch angle. The magnetic energy density of the turbulent magnetic field is given by

$$W(k_\parallel) = \frac{|\Delta B|^2}{8\pi}\frac{1}{\nu}\frac{1}{\delta\omega}\left|\frac{d\omega}{dk}\right|\exp\left(-\frac{(\omega-\omega_m)^2}{\delta\omega}\right). \tag{8}$$

Here, $|\Delta B|^2$ is the mean wave intensity, $\nu = \frac{\sqrt{\pi}}{2}\left[\mathrm{erf}\left(\frac{\omega_m-\omega_1}{\delta\omega}\right)+\mathrm{erf}\left(\frac{\omega_2-\omega_m}{\delta\omega}\right)\right]$ with erf being the error function. ω, ω_m, and $\delta\omega$ are the frequency of EMIC waves, the frequency of the maximum wave power and the bandwidth, respectively. ω_1 and ω_2 are the lower and upper cutoff frequencies.

Our estimates of local pitch angle scattering rates, $D_{\alpha\alpha}$, in Figure 4 are based on the realistic ion distributions and plasma and wave spectrum parameters. In comparison with the cold plasma result, the large differences indicate that hot plasma effects can change the scattering rates significantly. We note that the hot plasma correction may decrease the scattering rate magnitude, but enhance the resonant pitch angle range available for scattering (see panels a–f). In panels g–h, it is also evident that hot plasma effects can decrease (increase) the scattering rate for Event 1 (Event 2 and 3) for low-energy electrons but increase the scattering rate for higher-energy electrons during all cases. Changes in the scattering rate depend on the observed ion distribution and the wave spectrum in each case. Among all these parameters, the anisotropy, A_h, plays the most significant role in controlling the resonant pitch-angle range and the scattering rate magnitude. Although this parameter cannot always be determined (due to the absence of reliable plasma measurements for the majority of EMIC wave statistics), there is a direct relation between A_h and the maximum EMIC wave frequency: $A_{hp} = \omega_{\max}/(\Omega_p - \omega_{\max})$. Therefore, this parameter in Equation 6 can be substituted by the measurable EMIC wave characteristic, $\omega_{\max}$.

6. Conclusions

We have presented an analytical hot plasma model for EMIC wave dispersion relation and verified this model with numerical solutions based on observed EMIC wave parameters during three cases. Note that although we focused on proton-electron plasma, the model provided in Equations 3–6 can be applied to multi-ion (including heavy ions) plasma. The main conclusions of our study are:

1. The presented analytical model of hot plasma effects for EMIC waves outputs the wavenumber (and growth rate) in an excellent agreement with the numerical solutions (with a 10%–15% error). This model can be used to evaluate more precisely the diffusion coefficients and nonlinear wave-particle interactions.
2. The hot plasma effects significantly increase the minimum energy of electrons resonating with the most intense EMIC waves (waves with frequencies corresponding to the maximum growth rate), but can decrease the minimum resonant energy for the higher-frequency part of EMIC spectra corresponding to smaller wave intensity (marginally stable waves). Therefore, a proper evaluation of the minimum energy of electrons that undergo resonant scattering by EMIC waves requires investigation of the entire unstable wave frequency range.

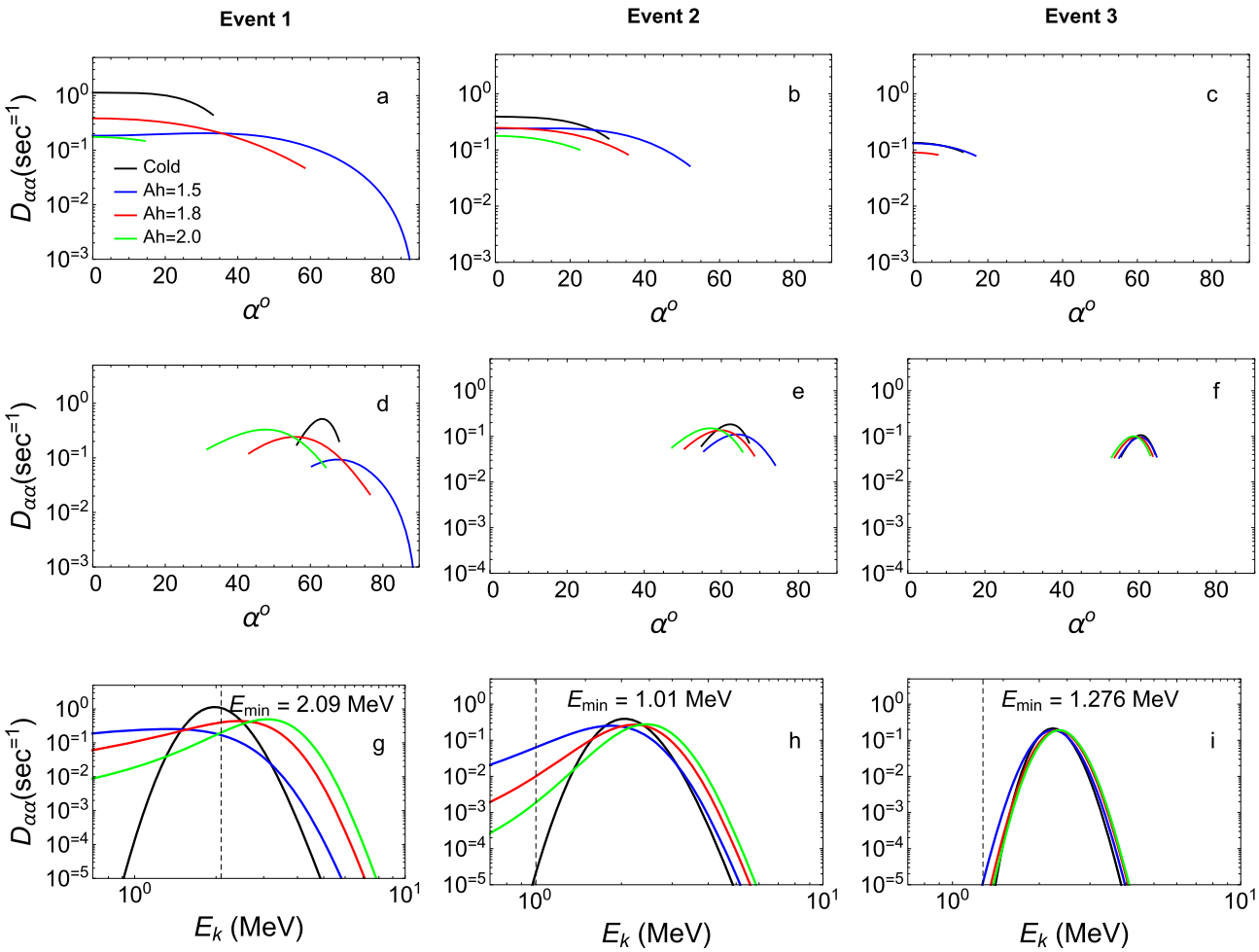

Figure 4. (a–c) Pitch angle scattering rates as a function of pitch angle in degrees ($\alpha°$) for 2 MeV (top panels) and (d–f) 5 MeV (middle panels) electrons and (g–i) as a function of energy for a fixed pitch angle at $\alpha = 5°$ (bottom panels) for events from Figure 1 based on fitted ion distributions and wave spectra given in Figure 2. Cold plasma case is shown in black, as well as the hot plasma case for three different anisotropy values: $A_{hp} = 1.5$ (blue), $A_{hp} = 1.8$ (red) and $A_{hp} = 2.0$ (green). The vertical dashed line represents the minimum resonant energy for each event.

3. The estimated pitch angle scattering rate based on the hot plasma model, realistic plasma and wave spectrum parameters show that the hot plasma effects significantly change the scattering rates and expand the electron pitch angle range for the interaction between EMIC and relativistic electrons.

Data Availability Statement

THEMIS data is available at http://themis.ssl.berkeley.edu/data/themis. Data analysis was done using SPEDAS V4.1 (Angelopoulos et al., 2019) available at https://spedas.org/.

Acknowledgments
We acknowledge support by NASA awards 80NSSC20K1270 and NSF grants AGS-2021749. We acknowledge NASA contract NAS5-02099 for use of data from the THEMIS mission. We thank K. H. Glassmeier, U. Auster, and W. Baumjohann for the use of FGM data provided under the lead of the Technical University of Braunschweig and with financial support through the German Ministry for Economy and Technology and the German Aerospace Center (DLR) under contract 50 OC 0302.

References

Albert, J. M., & Bortnik, J. (2009). Nonlinear interaction of radiation belt electrons with electromagnetic ion cyclotron waves. *Geophysical Research Letters*, *36*(12), 12110. https://doi.org/10.1029/2009GL038904

Angelopoulos, V. (2008). The THEMIS mission. *Space Science Reviews*, *141*(1–4), 5–34. https://doi.org/10.1007/s11214-008-9336-1

Angelopoulos, V., Cruce, P., Drozdov, A., Grimes, E. W., Hatzigeorgiu, N., King, D. A., et al. (2019). The Space Physics Environment Data Analysis System (SPEDAS). *Space Science Reviews*, *215*(1), 9. https://doi.org/10.1007/s11214-018-0576-4

Angelopoulos, V., McFadden, J. P., Larson, D., Carlson, C. W., Mende, S. B., Frey, H., et al. (2008). Tail reconnection triggering substorm onset. *Science*, *321*(5891), 931–935. https://doi.org/10.1126/science.1160495

Auster, H. U., Glassmeier, K. H., Magnes, W., Aydogar, O., Baumjohann, W., Constantinescu, D., et al. (2008). The THEMIS fluxgate magnetometer. *Space Science Reviews*, *141*(1–4), 235–264. https://doi.org/10.1007/s11214-008-9365-9

Bashir, M. F., Artemyev, A., Zhang, X.-J., & Angelopoulos, V. (2022). Energetic electron precipitation driven by the combined effect of ULF, EMIC, and whistler waves. *Journal of Geophysical Research*, *127*(1), e2021JA029871. https://doi.org/10.1029/2021JA029871

Bashir, M. F., & Ilie, R. (2018). A new N+ band of electromagnetic ion cyclotron waves in multi-ion cold plasmas. *Geophysical Research Letters*, *45*(19), 10150–10159. https://doi.org/10.1029/2018GL080280

Blum, L. W., Halford, A., Millan, R., Bonnell, J. W., Goldstein, J., Usanova, M., et al. (2015). Observations of coincident EMIC wave activity and duskside energetic electron precipitation on 18–19 January 2013. *Geophysical Research Letters*, *42*(14), 5727–5735. https://doi.org/10.1002/2015GL065245

Cai, B., Wu, Y., & Tao, X. (2020). Effects of nonlinear resonance broadening on interactions between electrons and whistler mode waves. *Geophysical Research Letters*, *47*(11), e87991. https://doi.org/10.1029/2020GL087991

Cao, J., Shprits, Y. Y., Ni, B., & Zhelavskaya, I. S. (2017). Scattering of ultra-relativistic electrons in the Van Allen radiation belts accounting for hot plasma effects. *Scientific Reports*, *7*(1), 17719. https://doi.org/10.1038/s41598-017-17739-7

Cao, X., Ni, B., Summers, D., Fu, S., Gu, X., & Shi, R. (2020). Hot plasma effects on the pitch-angle scattering rates of radiation belt electrons due to plasmaspheric hiss. *The Astrophysical Journal*, *896*(2), 118. https://doi.org/10.3847/1538-4357/ab9107

Capannolo, L., Li, W., Ma, Q., Chen, L., Shen, X. C., Spence, H. E., et al. (2019). Direct observation of sub-relativistic electron precipitation potentially driven by EMIC waves. *Geophysical Research Letters*, *46*(22), 12711–12721. https://doi.org/10.1029/2019GL084202

Capannolo, L., Li, W., Ma, Q., Shen, X. C., Zhang, X. J., Redmon, R. J., et al. (2019). Energetic electron precipitation: Multievent analysis of its spatial extent during EMIC wave activity. *Journal of Geophysical Research*, *124*(4), 2466–2483. https://doi.org/10.1029/2018JA026291

Chen, L., Thorne, R. M., & Bortnik, J. (2011). The controlling effect of ion temperature on EMIC wave excitation and scattering. *Geophysical Research Letters*, *38*(16), L16109. https://doi.org/10.1029/2011GL048653

Chen, L., Thorne, R. M., Bortnik, J., & Zhang, X.-J. (2016). Nonresonant interactions of electromagnetic ion cyclotron waves with relativistic electrons. *Journal of Geophysical Research*, *121*(10), 9913–9925. https://doi.org/10.1002/2016JA022813

Chen, L., Zhu, H., & Zhang, X. (2019). Wavenumber analysis of EMIC waves. *Geophysical Research Letters*, *46*(11), 5689–5697. https://doi.org/10.1029/2019GL082686

Denton, R. E., Ofman, L., Shprits, Y. Y., Bortnik, J., Millan, R. M., Rodger, C. J., et al. (2019). Pitch angle scattering of sub-MeV relativistic electrons by electromagnetic ion cyclotron waves. *Journal of Geophysical Research*, *124*(7), 5610–5626. https://doi.org/10.1029/2018JA026384

Drozdov, A. Y., Shprits, Y. Y., Usanova, M. E., Aseev, N. A., Kellerman, A. C., & Zhu, H. (2017). EMIC wave parameterization in the long-term VERB code simulation. *Journal of Geophysical Research*, *122*(8), 8488–8501. https://doi.org/10.1002/2017JA024389

Fried, B. D., & Conte, S. D. (1961). *The plasma dispersion function*. Academic Press. https://doi.org/10.1016/C2013-0-12176-9

Grach, V. S., & Demekhov, A. G. (2020). Precipitation of relativistic electrons under resonant interaction with electromagnetic ion cyclotron wave packets. *Journal of Geophysical Research*, *125*(2), e27358. https://doi.org/10.1029/2019JA027358

Hendry, A. T., Rodger, C. J., & Clilverd, M. A. (2017). Evidence of sub-MeV EMIC-driven electron precipitation. *Geophysical Research Letters*, *44*(3), 1210–1218. https://doi.org/10.1002/2016GL071807

Jun, C. W., Yue, C., Bortnik, J., Lyons, L. R., Nishimura, Y., & Kletzing, C. (2019). EMIC wave properties associated with and without injections in the inner magnetosphere. *Journal of Geophysical Research*, *124*(3), 2029–2045. https://doi.org/10.1029/2018JA026279

Karimabadi, H., Krauss-Varban, D., & Terasawa, T. (1992). Physics of pitch angle scattering and velocity diffusion 1. Theory. *Journal of Geophysical Research*, *97*(A9), 13853–13864. https://doi.org/10.1029/92JA00997

Kubota, Y., Omura, Y., & Summers, D. (2015). Relativistic electron precipitation induced by EMIC-triggered emissions in a dipole magnetosphere. *Journal of Geophysical Research*, *120*(6), 4384–4399. https://doi.org/10.1002/2015JA021017

McFadden, J. P., Carlson, C. W., Larson, D., Ludlam, M., Abiad, R., Elliott, B., et al. (2008). The THEMIS ESA plasma instrument and in-flight calibration. *Space Science Reviews*, *141*(1–4), 277–302. https://doi.org/10.1007/s11214-008-9440-2

Millan, R. M., & Thorne, R. M. (2007). Review of radiation belt relativistic electron losses. *Journal of Atmospheric and Solar-Terrestrial Physics*, *69*(3), 362–377. https://doi.org/10.1016/j.jastp.2006.06.019

Ni, B., Cao, X., Shprits, Y. Y., Summers, D., Gu, X., Fu, S., & Lou, Y. (2018). Hot plasma effects on the cyclotron-resonant pitch-angle scattering rates of radiation belt electrons due to EMIC waves. *Geophysical Research Letters*, *45*(1), 21–30. https://doi.org/10.1002/2017GL076028

Ni, B., Cao, X., Zou, Z., Zhou, C., Gu, X., Bortnik, J., et al. (2015). Resonant scattering of outer zone relativistic electrons by multiband EMIC waves and resultant electron loss time scales. *Journal of Geophysical Research*, *120*(9), 7357–7373. https://doi.org/10.1002/2015JA021466

Nishimura, Y., Bortnik, J., Li, W., Thorne, R. M., Ni, B., Lyons, L. R., et al. (2013). Structures of dayside whistler-mode waves deduced from conjugate diffuse aurora. *Journal of Geophysical Research*, *118*(2), 664–673. https://doi.org/10.1029/2012JA018242

Shprits, Y. Y., Thorne, R. M., Friedel, R., Reeves, G. D., Fennell, J., Baker, D. N., & Kanekal, S. G. (2006). Outward radial diffusion driven by losses at magnetopause. *Journal of Geophysical Research*, *111*(A11), 11214. https://doi.org/10.1029/2006JA011657

Silin, I., Mann, I. R., Sydora, R. D., Summers, D., & Mace, R. L. (2011). Warm plasma effects on electromagnetic ion cyclotron wave MeV electron interactions in the magnetosphere. *Journal of Geophysical Research*, *116*(A5), A05215. https://doi.org/10.1029/2010JA016398

Sorathia, K. A., Ukhorskiy, A. Y., Merkin, V. G., Fennell, J. F., & Claudepierre, S. G. (2018). Modeling the depletion and recovery of the outer radiation belt during a geomagnetic storm: Combined MHD and test particle simulations. *Journal of Geophysical Research*, *123*(7), 5590–5609. https://doi.org/10.1029/2018JA025506

Summers, D. (2005). Quasi-linear diffusion coefficients for field-aligned electromagnetic waves with applications to the magnetosphere. *Journal of Geophysical Research*, *110*, A08213. https://doi.org/10.1029/2005JA011159

Summers, D., & Thorne, R. M. (2003). Relativistic electron pitch-angle scattering by electromagnetic ion cyclotron waves during geomagnetic storms. *Journal of Geophysical Research*, *108*(A4), 1143. https://doi.org/10.1029/2002JA009489

Thorne, R. M., & Kennel, C. F. (1971). Relativistic electron precipitation during magnetic storm main phase. *Journal of Geophysical Research*, *76*(19), 4446–4453. https://doi.org/10.1029/JA076i019p04446

Turner, D. L., Shprits, Y., Hartinger, M., & Angelopoulos, V. (2012). Explaining sudden losses of outer radiation belt electrons during geomagnetic storms. *Nature Physics*, *8*(3), 208–212. https://doi.org/10.1038/nphys2185

Yoon, P. H., Summers, D., Seough, J. J., Kim, K. H., & Lee, D. H. (2011). Finite-beta effects on quasi-linear diffusion coefficients. *Journal of Geophysical Research*, *116*, A12214. https://doi.org/10.1029/2011JA017070

Zhang, X. J., Mourenas, D., Shen, X. C., Qin, M., Artemyev, A. V., Ma, Q., et al. (2021). Dependence of relativistic electron precipitation in the ionosphere on EMIC wave minimum resonant energy at the conjugate equator. *Journal of Geophysical Research*, *126*(5), e2021JA029193. https://doi.org/10.1029/2021JA029193